

Surface- and pressure-induced bulk Kondo breakdown in SmB<sub>6</sub>HPSTAR  
594-2018K. Chen,<sup>1,\*</sup> T-C. Weng,<sup>2</sup> G. Schmerber,<sup>3</sup> V. N. Gurin,<sup>4</sup> J.-P. Kappler,<sup>1</sup> Q. Kong,<sup>1</sup> F. Baudelet,<sup>1</sup> A. Polian,<sup>1,5</sup> and L. Nataf<sup>1</sup><sup>1</sup>Synchrotron SOLEIL, L'Orme des Merisiers, Saint-Aubin-BP48, 91192 Gif-sur-Yvette Cedex, France<sup>2</sup>Center for High Pressure Science & Technology Advanced Research, 1690 Cailun Road, 201203 Shanghai, China<sup>3</sup>IPCMS, CNRS-Université de Strasbourg, 23 rue du Loess, BP 43, 67034 Strasbourg Cedex 2, France<sup>4</sup>Ioffe Institute, Russian Academy of Sciences, St. Petersburg 194021, Russia<sup>5</sup>IMPMC, Sorbonne Université, C.N.R.S. UMR 7590, 4 Place Jussieu, 75005 Paris, France

(Received 2 March 2018; revised manuscript received 13 June 2018; published 29 June 2018)

Motivated by the prediction of surface Kondo breakdown in topological Kondo insulators, we investigated the valence and magnetism of SmB<sub>6</sub> with x-ray absorption and magnetic circular dichroism at the Sm  $M_{4,5}$  and  $L_2$  edges with surface and bulk sensitivity, respectively. A higher Sm valence state at the surface and in the bulk under pressure indicates the surface- and pressure-induced bulk Kondo breakdown. We confirmed the different magnetization origin from the surface ( $f$  electron) to the bulk ( $d$  electron) and ascertained the direct relationship between the disappearance of the Sm  $L_2$ -edge x-ray magnetic circular dichroism signal and the closure of the  $d$ - $f$  hybridization gap in SmB<sub>6</sub> bulk under pressure, paving the way for further investigations of the Kondo insulators. Above  $P_c = 8.5$  GPa, a more localized  $4f$  state with higher valence and the disappearing of the  $5d$  magnetism are observed, suggesting the closure of the hybridization gap in the bulk.

DOI: [10.1103/PhysRevB.97.235153](https://doi.org/10.1103/PhysRevB.97.235153)

## I. INTRODUCTION

The Kondo insulator SmB<sub>6</sub> was considered as a good candidate material of topological Kondo insulator [1–6]. The long-standing mysterious low-temperature-resistance plateau can be well explained with the topologically protected metallic surface states within a hybridization gap hosted in the topological Kondo insulator [7–14]. In SmB<sub>6</sub>, the strong hybridization of the low-lying localized  $4f$  electronic bands with a broad  $5d$  conduction band [15,16] via the Kondo effect gives rise to a hybridization gap of the order of 20 meV, resulting in the screening of localized  $4f$  magnetic moments. The strong hybridization also leads to a mixture of the Sm<sup>2+</sup> ( $4f^6$ ) and Sm<sup>3+</sup> ( $4f^5$ ) configurations, with the electronic structure described by the Hund's rule ground states with total orbital momenta of  $J = 0$  and  $5/2$ , respectively. The bulk and surface electronic properties have been investigated using a wide range of experimental methods, high-pressure x-ray-absorption spectroscopy experiments [17,18], scanning tunneling spectroscopy [19–21], angle-resolved photoelectron spectroscopy [22–24], hard x-ray photoelectron spectroscopy [25,26], and resonant soft x-ray reflectometry [27] providing additional confirmation of surface states in SmB<sub>6</sub>.

Recently, a Kondo breakdown scenario was proposed based on the reduced screening of the local moments at the surface and the marked reduction in the surface Kondo temperature  $T_K^s \sim T_K/10$  [28,29]. With the reduction of nearest-neighbor sites of the Sm<sup>3+</sup> ions on the surface, the screening of local moments is either shifted to lower temperatures [7,8,10,21], or disappears completely [13]. A change in Sm valence at the

surface has been reported from x-ray-absorption spectroscopy (XAS) and x-ray magnetic circular dichroism (XMCD), which is claimed to be the definitive proof of changes in the electronic structure at the surface of SmB<sub>6</sub> [11]. A surface dominated conduction at 240 K has been achieved in epitaxial SmB<sub>6</sub> films with a small 0.7% tensile strain enhanced  $d$ - $f$  hybridization [30], shedding light on the tuning of the ground state of the compound. For bulk SmB<sub>6</sub>, pressure-induced long-range magnetic ordering was reported in the metallic state above a critical pressure  $P_c$  from nuclear forward scattering and specific-heat measurements [31], and the pressure-induced localization of  $4f$  states was supported by <sup>11</sup>B-NMR results [32].

Different magnetic properties are expected for the metallic surface and the insulator bulk of SmB<sub>6</sub>. Considering the surface Kondo breakdown scenario, the surface magnetism is mainly due to the  $4f$  electrons. On the contrary, as recently reported from inelastic neutron-scattering investigations, the  $5d$  magnetic contribution [33] is expected in the bulk due to the screening of the  $4f$  moments. Under pressure, the hybridization gap in bulk SmB<sub>6</sub> will be closed, resulting in the more localized  $4f$  electrons and less Sm ions with Sm<sup>2+</sup> configuration. To validate the proposed Kondo breakdown scenario, in this paper we report the surface and bulk electronic and magnetic properties of SmB<sub>6</sub>, investigated with XAS and XMCD at Sm  $M_{4,5}$  edges, and Sm  $L_2$  edge at  $T = 8$  K with pressure up to 26 GPa. We observed the obvious  $4f$  magnetism with a higher valence of  $\nu = 2.74(3)$  ( $T = 4$  K) at the surface and a very small  $4f$  bulk magnetism with the lower valence of  $\nu = 2.55(3)$  ( $T = 8$  K). The  $5d$  magnetic contribution of bulk SmB<sub>6</sub> is clearly observed from the Sm  $L_2$ -edge XMCD spectra, and disappears around  $\sim 7$ – $10$  GPa. These results confirmed the Kondo breakdown scenario in SmB<sub>6</sub>, accompanied by a reduced  $d$ - $f$  hybridization in both cases.

\*kaichen.hzg@gmail.com

## II. SAMPLES AND EXPERIMENTAL SET-UP

As a congruently melting compound [34–36],  $\text{SmB}_6$  has been prepared using the floating zone melting technique, by sealing a quartz ampoule with an excess of Sm, due to the higher pressure of Sm vapor than that of boron, under a pressurized gas atmosphere of pure Ar. Single phase  $\text{SmB}_6$  powder was characterized by laboratory x-ray diffraction (XRD) measurement which leads to a lattice parameter  $a = 4.1341(5)$  Å, with an average size of the crystallites of the order of 200 nm.

$\text{SmB}_6$  powder was compressed into pellets for soft x-ray measurements. XAS and XMCD spectra at the Sm  $M_{4,5}$  edges were measured from 4 to 300 K using the surface sensitive total electron yield (TEY) and bulk sensitive fluorescence yield (FY) mode with a normal incidence configuration. However, the “surface” defined here refers to the electron escaping length of the order of  $\sim 2$ –5 nm while the “bulk” is related to a thickness 10 times higher. The XMCD spectra were carried out using x rays of circular right (CR) and left (CL) polarizations with a magnetic field of  $\mu_0 H = \pm 6.5$  T applied along the beam, recorded as  $\sigma^+ - \sigma^-$ , where  $\sigma^+$  and  $\sigma^-$  denote the absorption cross section for right and left circular polarized x rays. A self-absorption correction procedure has been made based on the Fluo algorithm in the ATHENA analysis software [37] for the bulk XAS and XMCD spectra recorded FY-XAS. The XAS and XMCD spectra at the Sm  $L_2$ - edge have been performed to probe the pressure-dependent local electronic configuration and  $5d$  electron magnetism of Sm atoms.  $\text{SmB}_6$  powder, together with the pressure transmitting medium silicon oil, was pressurized up to 26 GPa in a diamond-anvil cell (DAC). The pressure was measured using the ruby fluorescence scale. XMCD was obtained through the difference of XAS spectra measured under a magnetic field of  $\mu_0 H = 1.3$  T applied parallel or antiparallel to the beam helicity. The spectra of Sm  $M_{4,5}$  and  $L_2$  edge were recorded at the DEIMOS [38] and ODE beamlines [39] respectively, at synchrotron SOLEIL, France.

## III. RESULTS AND DISCUSSION

The XAS spectra of Sm  $M_{4,5}$  edges, collected simultaneously using TEY and FY modes at  $T = 4$  K, are shown in Fig. 1(a). The Sm  $3d$ - $4f$  transition is split into a  $3d_{5/2}$  and a  $3d_{3/2}$  branch due to the spin-orbit interaction. Each of these branches is a mixture of the  $\text{Sm}^{2+}$  ( $4f^6$ ) and  $\text{Sm}^{3+}$  ( $4f^5$ ) components. The shoulder and main peak positions of the Sm  $M_5$  edge, addressed to be the contribution from  $\text{Sm}^{2+}$  and  $\text{Sm}^{3+}$ , are well reproduced from atomic multiplet simulation using CTM4XAS code [40], with the electrostatic and exchange parameters scaled down to 80% of the atomic Hartree-Fock value, and convoluted with a Lorentzian function for lifetime broadening and a Gaussian to account for the instrumental resolution. The shoulder in the bulk spectra is stronger than that in the surface spectra, indicating a higher  $\text{Sm}^{2+}$  contribution and a lower Sm valence state. We investigate whether the spectrum can be interpreted using the spectra of  $\text{Sm}^{2+}$  and  $\text{Sm}^{3+}$  from the full multiplet simulation shown in Fig. 1(a). A weighted sum of TEY- and FY-XAS (4 K) has been built and compared to the experimental spectra, shown in Figs. 1(b) and 1(c). The weighted sum (27%  $\text{Sm}^{2+}$  and 73%  $\text{Sm}^{3+}$  for surface,

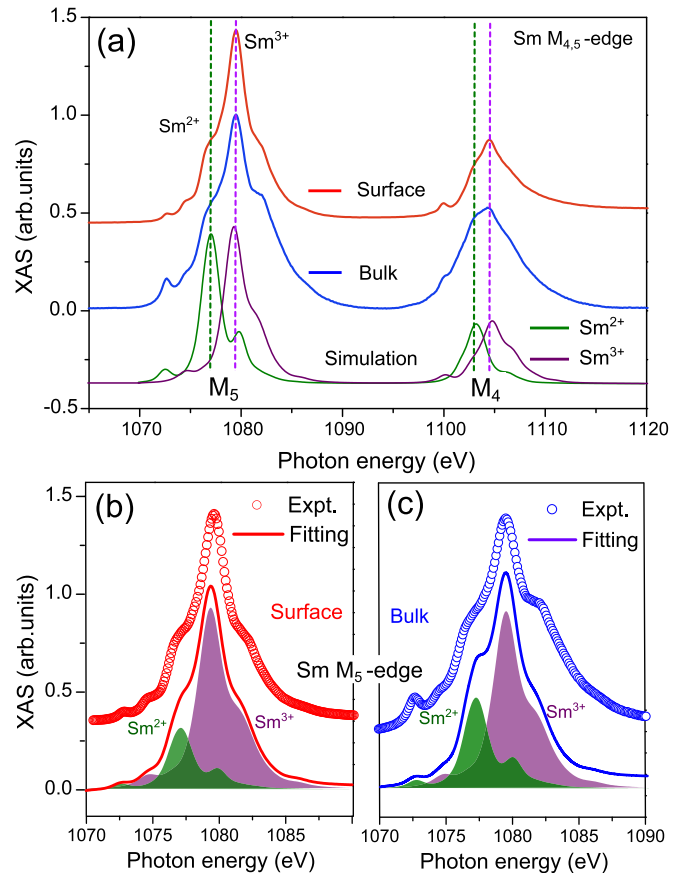


FIG. 1. (a) XAS of  $\text{SmB}_6$  at Sm  $M_{4,5}$  edges of TEY (red curve) and FY-XAS (blue curve) at  $T = 4$  K, as well as the spectra of  $\text{Sm}^{2+}$  and  $\text{Sm}^{3+}$  from atomic multiplet calculation. The surface (b) and bulk (c) XAS spectra can be well fitted with the combination of the spectra of  $\text{Sm}^{2+}$  and  $\text{Sm}^{3+}$  from atomic multiplet calculation.

and 35%  $\text{Sm}^{2+}$  and 65%  $\text{Sm}^{3+}$  for bulk) of the simulated curves describe the  $\text{SmB}_6$  spectrum very well. The Sm mean valence in  $\text{SmB}_6$  can be derived from  $\nu = 2 + I(f^5)/[I(f^5) + I(f^6)]$ , where  $I(f^5)$  and  $I(f^6)$  denote the integrated intensities of the  $\text{Sm}^{3+}$  and  $\text{Sm}^{2+}$  components. The deduced Sm valences are 2.73(3) and 2.65(5) for the surface and bulk  $\text{SmB}_6$ , respectively. Zabolotnyy *et al.*, reported that the highly polar (001) surface undergoes substantial chemical and valence reconstruction, resulting a  $\text{Sm}^{3+}$  dominated subsurface region [27]. Here we have small particles (several micrometers) that give a rather rough surface mixed with different crystal surfaces. Our results indicate that the surface valence reconstruction may be formed on all surfaces of  $\text{SmB}_6$ .

Even after the self-absorption correction for the FY XAS, the valence of Sm still can be overestimated [41]. In order to extract the valence of the Sm in the bulk under pressure, experimental Sm  $L_2$  edge XAS spectra are recorded and shown in Fig. 2(a) ( $T = 8$  K,  $P = 0.6$ –26 GPa). The  $\text{Sm}^{2+}$  contribution, marked with a dashed line as the shoulder in Fig. 2(a), decreases with pressure which indicates the increase of the Sm valence. The spectra are analyzed by assigning identical line shapes (with core hole lifetime broadening) to the  $\text{Sm}^{2+}$  and  $\text{Sm}^{3+}$  contribution in the spectra, each with a proportionality tanh-type background, as shown in Figs. 2(b)

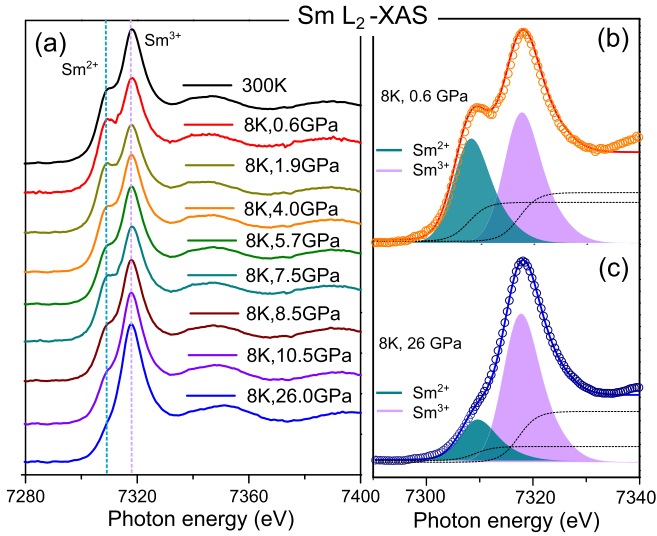


FIG. 2. (a) XAS of Sm  $L_2$  edges at 8 K under pressure up to 26 GPa, and the spectrum recorded at 300 K for comparison. The  $L_2$  edge XAS at 8 K,  $P = 0.6$  (b) and 26.0 GPa (c) were well fitted with the combination of the spectra of  $\text{Sm}^{2+}$  and  $\text{Sm}^{3+}$  with identical line shapes, with the tanh-type background.

and 2(c) for pressure of 0.6 and 26.0 GPa, respectively. Derived from the fitting procedure, the Sm ion has a lower mean valence of  $\nu = 2.55(3)$  at  $T = 8$  K and  $P = 0.6$  GPa and a much higher mean valence of  $\nu = 2.78(3)$  when the pressure increased up to 26.0 GPa. This bulk Sm valence under pressure ( $\nu = 2.78$ ) is even higher than the surface Sm valence ( $\nu = 2.73$ ) at ambient pressure determined from Sm  $M_{4,5}$  XAS.

Applying the fitting procedure, we extracted the Sm mean valence as a function of temperature and pressure (Fig. 3). As shown in the inset, the mean valence of surface Sm ions is higher compared to the value of the bulk Sm ions through the

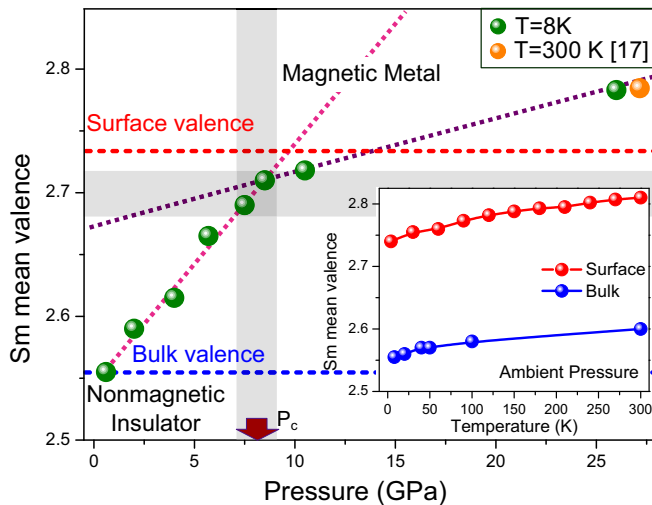


FIG. 3. Pressure dependence of the Sm mean valence in  $\text{SmB}_6$ . The inset shows the temperature dependence of the surface and bulk Sm mean valence in  $\text{SmB}_6$ , respectively. The grey area shows the region of nonmagnetic insulator to magnetic metal transition. Error bars are smaller than the points.

whole temperature range, and both of them increase gradually with temperature. At ambient pressure, the valence of the Sm ions changes slightly from  $\nu = 2.55(3)$  to  $2.60(3)$  in bulk and from  $\nu = 2.73(3)$  to  $2.80(3)$  on surfaces from  $T = 4$  to 300 K. In general, our findings for the bulk Sm valence and its temperature dependence are consistent with the results reported in earlier Sm  $L_{2,3}$ -edge XAS experiments [42]. A relative higher valence state ( $\nu = 2.73$ ) is obtained at the surface, consistent with the surface Kondo breakdown scenario, in contrast to the entire surface  $\text{Sm}^{3+}$  reported in [11]. At  $T = 8$  K, a quick enhancement of the valence was observed under pressure from  $\nu = 2.55$  at 0.6 GPa to  $\nu = 2.70$  at  $P_c \sim 8$  GPa, followed by a slow valence increase to  $\nu = 2.78$  at 26 GPa, across the level of the surface valence value of  $\nu = 2.73$ .  $\text{SmB}_6$  becomes magnetically ordered below 12 K [31,43] once the insulating gap closes by 5–10 GPa [44,45], with a Sm mean valence of  $\nu \sim 2.69(3)$  [17] (marked as the grey area in Fig. 3). In the Kondo breakdown regime above  $\sim 10$  GPa, the Sm valence remains unchanged with temperature in bulk  $\text{SmB}_6$ . When comparing the present experimental results (8 K) with the previous data recorded at 300 K [17] at  $\sim 26$  GPa, we found that the Sm valence remains unchanged, consistent with the pressure-induced Kondo breakdown scenario.

The higher Sm mean valence indicates a relative weaker hybridization between  $4f$  and  $5d$  states on the  $\text{SmB}_6$  surface than in the bulk at ambient pressure, and a weaker hybridization in the bulk under pressure. In both cases, the screening of  $4f$  local moments will be suppressed. This will make the  $4f$  magnetization the main magnetic contribution at the surface or in the bulk under pressure. In the bulk at ambient pressure, the local  $4f$  magnetization is highly screened by the conduction electrons, resulting in the paramagnetic ground state. Hence the magnetic contributions from the  $5d$  electrons is not negligible. The  $5d$  magnetization as well as the reduced  $4f$  magnetization in bulk  $\text{SmB}_6$  were observed from the XAS and XMCD of Sm at  $L_2$  edge and  $M_{4,5}$  edge.

Based on the surface Kondo breakdown scenario, the surface magnetization is expected to be much stronger compared to the bulk with normal Kondo screening of  $4f$  magnetization. To confirm the proposed reduction of Kondo screening at the surface in more detail, we collected Sm  $M_{4,5}$ -edge XMCD spectra simultaneously for surface (red curve) and bulk (blue curve) at  $T = 4$  K and  $\mu_0 H = 6.5$  T [Fig. 4(a) inset]. According to the nonmagnetic  $J = 0$  singlet ( $4f^6$ ) of  $\text{Sm}^{2+}$ , the XMCD signal comes from the  $\text{Sm}^{3+}$  contribution at the surface with a shape similar to that observed in  $\text{SmAl}_2$  [46] and  $\text{Sm}_{0.974}\text{Gd}_{0.02}\text{Al}_2$  [47]. Several phenomena related to the multiplet structure of the intermediate state may occur which render FY XMCD different from the true XMCD spectrum at the  $M_{4,5}$  edge of rare earths [41]. Thus, the main qualitative observation for the bulk is a reduced XMCD intensity, roughly  $1/4$ , as compared to the XMCD on the surface, indicating a much smaller  $4f$  contributed magnetization in the bulk  $\text{SmB}_6$ . Besides, the bulk XMCD spectrum from the FY mode shows a negative signal at the Sm  $M_4$  edge, in contrast with the positive signal at the surface. Those results state clearly that the  $4f$  magnetic contribution, which dominates the surface magnetism, is strongly reduced in the bulk.

Sm  $L_2$ -edge XAS and XMCD spectra are presented in Fig. 4(b), recorded at 40 K,  $P = 0.6$  GPa, and  $\mu_0 H = 1.3$  T.

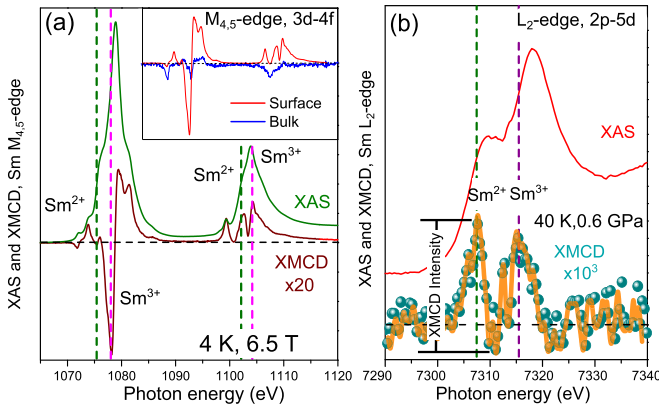


FIG. 4. (a) XAS and XMCD of Sm at  $\text{SmB}_6$  surface at  $M_{4,5}$  edge ( $3d-4f$ ) at  $T = 4$  K, 6.5 T, ambient pressure, and (b)  $L_2$  edge ( $2p-5d$ ) at 8 K, 1.3 T, 0.6 GPa for bulk  $\text{SmB}_6$ . The comparison of the Sm  $M_{4,5}$  XMCD spectra from TEY XAS (red curve) and FY XAS (blue curve) is shown as inset in (a).

Two well defined peaks are clearly present in both XAS and XMCD spectra. The quadrupolar contribution as a result of  $4f/5d$  hybridization is strong in Sm  $L_3$  edge but highly reduced in  $L_2$  edge XMCD spectra in  $\text{SmN}$  [48]. Thus these spectral features with separated peaks from  $\text{Sm}^{2+}$  and  $\text{Sm}^{3+}$  in the XANES and XMCD signal were related to the dipolar contribution from the  $2p-5d$  excitations. The peak positions of the XMCD spectra are several eV below the XANES peaks, similar to that observed in  $\text{Sm}_{1-x}\text{Gd}_x\text{Al}_2$  [49].

The magnetization curve of bulk  $\text{SmB}_6$  as a function of temperature measured with a magnetometer property measurement system superconducting quantum interference device vibrating-sample magnetometer (Quantum Design) is shown in Fig. 5(a), under zero-field-cooling (ZFC) or field-cooling (FC) conditions in an applied field of  $\mu_0 H = 2$  T. The bulk magnetization value is in good agreement with Ref. [11].

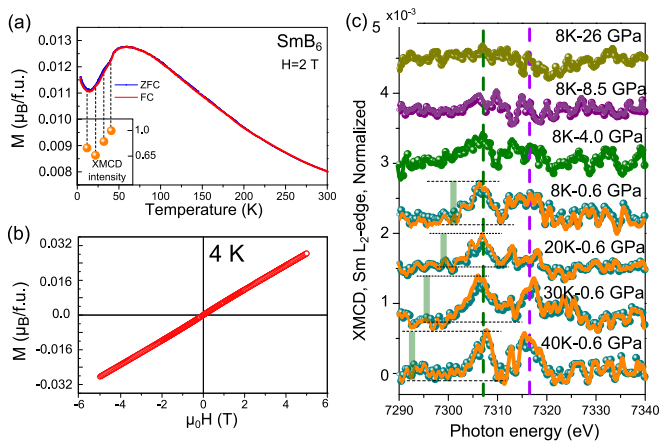


FIG. 5. (a) Magnetization and (b) paramagnetic magnetic curve  $M(H)$  loop at 4 K. (c) Temperature- and pressure-dependent Sm  $L_2$ -edge XMCD spectra of bulk  $\text{SmB}_6$ , normalized to the XAS intensity. This  $L_2$ -edge XMCD intensity follows the temperature behavior of the bulk magnetization as shown in (a) inset, and disappears when  $P > P_c \sim 8.5$  GPa.

The paramagnetic curve with no observable hysteresis in the  $M(H)$  loop of  $\text{SmB}_6$  taken at  $T = 4$  K is shown in Fig. 5(b). The temperature- and pressure-dependent Sm  $L_2$ -edge XMCD spectra of bulk  $\text{SmB}_6$  are shown in Fig. 5(c), normalized to the XAS intensity. The bulk magnetism shows a maximum around 50 K and a dip at around 15 K [Fig. 5(a)]. The normalized temperature-dependent intensity of the Sm  $L_2$ -edge XMCD spectra follows the similar temperature behavior as the bulk magnetization, as shown in Fig. 5(a) inset. It indicates the direct relationship between the  $5d$  electrons and the bulk paramagnetic magnetization in  $\text{SmB}_6$  at ambient pressure. At fixed temperature of 8 K, the intensity of the XMCD spectra decreases under pressure and disappears when  $P > P_c \sim 8.5$  GPa.

The  $\text{SmB}_6$  surface magnetism can be estimated, based on the enhanced XMCD spectra shown in Fig. 4(a), to compare with the bulk magnetization curve in Figs. 5(a) and 5(b). The XMCD sum rules can yield separate values of  $M_{S_z}$  and  $M_{L_z}$  based on the integration of the XAS and XMCD spectra, with a correction factor of  $X_I/X_E = 3$  of the spin sum rule due to the  $jj$  mixing of the two spin-orbit split states of  $\text{Sm}^{3+}$  [46,47,50]. We obtain the orbital and spin moments,  $M_L = 0.10(2)\mu_B$  and  $M_S = -0.03(1)\mu_B$ , which lead to a magnetic moment at the surface of  $0.07(3)\mu_B$ , at  $T = 4$  K and  $\mu_0 H = 6.5$  T, compared to the bulk magnetization of  $\sim 0.035(5)\mu_B$  shown in Fig. 5(b) (extrapolated to 6.5 T). The surface magnetic moment is twice enhanced compared to the bulk magnetism. Since the sum rule is not valid for the FY-mode XMCD spectra, the reduced intensity indicates that the  $4f$  states bear a small magnetic moment in the bulk.

The highly reduced  $4f$  magnetization indicates that the bulk magnetization of  $0.035(5)\mu_B$  mainly comes from the  $5d$  electron contribution, which is parallel to the applied magnetic field. Considering the ferromagnetic coupling between the spin magnetic moments of  $4f$  and  $5d$  electrons, the  $4f$  spin in bulk  $\text{SmB}_6$  is parallel aligned along the magnetic field. In contrast, at the surface, the  $4f$  orbital and spin moments are parallel and antiparallel to the magnetic field, respectively. The Sm  $4f$  spin magnetization changes its direction from the surface to the bulk, as observed in Fig. 4(a) inset, with opposite sign of the XMCD spectra from the surface and bulk using TEY and FY modes, respectively. Pressure-induced long-range magnetic ordering as well as the localization of Sm  $4f$  electrons have been expected from the pressure-induced Kondo breakdown scenario in  $\text{SmB}_6$  bulk. In this scenario, the magnetization in the bulk is dominated by the more localized  $4f$  electrons while the contribution from the  $5d$  electrons is reduced from the closed hybridization gap under pressure. The  $4f-5d$  hybridization in  $\text{SmB}_6$  under pressure is directly related to the Sm  $L_2$ -edge XMCD spectra, similar to the relationship observed in uranium compounds ( $\text{UCu}_2\text{Si}_2$  and  $\text{UMn}_2\text{Si}_2$ ) between the  $5f-6d$  hybridization and the U  $L_3$ -edge XMCD spectra [51]. Besides, a magnetically ordered state with a saturated moment of  $0.5\mu_B$  and an ordering temperature of 12 K was observed from high-pressure  $^{149}\text{Sm}$  nuclear forward scattering up to 26 GPa [31]. The vanishing XMCD signal above 8 GPa here indicates that the magnetic order of  $\text{SmB}_6$  should be of the antiferromagnetic type with no net Sm magnetization, since the ferromagnetic ordering of Sm  $4f$  moments will result in  $5d$  magnetization via intra-atomic exchange and this

ferromagnetism scenario can be ruled out by our experimental results.

#### IV. CONCLUSION

We conclude that the recently proposed surface- and pressure-induced bulk Kondo breakdown in Kondo insulator  $\text{SmB}_6$  are confirmed by XAS and XMCD spectra at the Sm  $M_{4,5}$  edge and  $L_2$  edge. Due to the reduced Kondo screening, as well as the  $d$ - $f$  hybridization, Sm ions at the surface have higher valence states and strongly enhanced magnetization of  $4f$  states compared to the Sm ions in the bulk. A transition from nonmagnetic insulator to magnetic metal has been observed with the Sm valence increase up to

$\nu = 2.78$  at 26 GPa at  $T = 8$  K. Bulk Sm ions lose their  $5d$  electron magnetization under pressure for  $P > P_c = 8.5$  GPa, entering the long-range magnetic ordering state dominated by the localized  $4f$  magnetization. We observed the direct relationship between the disappearance of the Sm  $L_2$ -edge XMCD signal and the closed  $d$ - $f$  hybridization gap in  $\text{SmB}_6$  bulk under pressure, demonstrating the potentiality of this methodology to investigate other Kondo insulators.

#### ACKNOWLEDGMENT

We acknowledge Synchrotron-Soleil for provision of synchrotron radiation facilities.

- 
- [1] M. Dzero, K. Sun, V. Galitski, and P. Coleman, *Phys. Rev. Lett.* **104**, 106408 (2010).
- [2] T. Takimoto, *J. Phys. Soc. Jpn.* **80**, 123710 (2011).
- [3] M. Dzero, K. Sun, P. Coleman, and V. Galitski, *Phys. Rev. B* **85**, 045130 (2012).
- [4] F. Lu, J. Z. Zhao, H. Weng, Z. Fang, and X. Dai, *Phys. Rev. Lett.* **110**, 096401 (2013).
- [5] M. Dzero and V. Galitski, *J. Exp. Theor. Phys.* **117**, 499 (2013).
- [6] V. Alexandrov, M. Dzero, and P. Coleman, *Phys. Rev. Lett.* **111**, 226403 (2013).
- [7] D. J. Kim, S. Thomas, T. Grant, J. Botimer, Z. Fisk, and J. Xia, *Sci. Rep.* **3**, 3150 (2013).
- [8] S. Wolgast, C. Kurdak, K. Sun, J. W. Allen, D.-J. Kim, and Z. Fisk, *Phys. Rev. B* **88**, 180405(R) (2013).
- [9] X. Zhang, N. P. Butch, P. Syers, S. Ziemak, R. L. Greene, and J. Paglione, *Phys. Rev. X* **3**, 011011 (2013).
- [10] D. J. Kim, J. Xia, and Z. Fisk, *Nat. Mater.* **13**, 466 (2014).
- [11] W. A. Phelan, S. M. Koohpayeh, P. Cottingham, J. W. Freeland, J. C. Leiner, C. L. Broholm, and T. M. McQueen, *Phys. Rev. X* **4**, 031012 (2014).
- [12] S. Thomas, D. J. Kim, S. B. Chung, T. Grant, Z. Fisk, and J. Xia, *Phys. Rev. B* **94**, 205114 (2016).
- [13] Y. Nakajima, P. Syers, X. Wang, R. Wang, and J. Paglione, *Nat. Phys.* **12**, 213 (2016).
- [14] Q. Wu and L. Sun, *Rep. Prog. Phys.* **80**, 112501 (2017).
- [15] G. Aeppli and Z. Fisk, *Comments Condens. Matter Phys.* **16**, 155 (1992).
- [16] P. W. Anderson, *Adv. Phys.* **49**, 257 (2000).
- [17] N. P. Butch, J. Paglione, P. Chow, Y. Xiao, C. A. Marianetti, C. H. Booth, and J. R. Jeffries, *Phys. Rev. Lett.* **116**, 156401 (2016).
- [18] L. Sun and Q. Wu, *Rep. Prog. Phys.* **79**, 084503 (2016).
- [19] S. Röβler, T.-H. Jang, D.-J. Kim, L. H. Tjeng, Z. Fisk, F. Steglich, and S. Wirth, *Proc. Natl. Acad. Sci. USA* **111**, 4798 (2014).
- [20] W. Ruan, C. Ye, M. Guo, F. Chen, X. Chen, G. M. Zhang, and Y. Wang, *Phys. Rev. Lett.* **112**, 136401 (2014).
- [21] L. Jiao, S. Röβler, D.-J. Kim, L. H. Tjeng, Z. Fisk, F. Steglich, and S. Wirth, *Nat. Commun.* **7**, 13762 (2016).
- [22] Z.-H. Zhu, A. Nicolaou, G. Levy, N. P. Butch, P. Syers, X. F. Wang, J. Paglione, G. A. Sawatzky, I. S. Elfimov, and A. Damascelli, *Phys. Rev. Lett.* **111**, 216402 (2013).
- [23] M. Neupane, N. Alidoust, S.-Y. Xu, T. Kondo, Y. Ishida, D.-J. Kim, C. Liu, I. Belopolski, Y. J. Jo, T.-R. Chang, H.-T. Jeng, T. Durakiewicz, L. Balicas, H. Lin, A. Bansil, S. Shin, Z. Fisk, and M. Z. Hasan, *Nat. Commun.* **4**, 2991 (2013).
- [24] J. Jiang, S. Li, T. Zhang, Z. Sun, F. Chen, Z. R. Ye, M. Xu, Q. Q. Ge, S. Y. Tan, X. H. Niu, M. Xia, B. P. Xie, Y. F. Li, X. H. Chen, H. H. Wen, and D. L. Feng, *Nat. Commun.* **4**, 3010 (2013).
- [25] P. Lutz, M. Thees, T. R. F. Peixoto, B. Y. Kang, B. K. Cho, C. H. Min, and F. Reinert, *Philos. Mag.* **96**, 3307 (2016).
- [26] Y. Utsumi, D. Kasinathan, K.-T. Ko, S. Agrestini, M. W. Haverkort, S. Wirth, Y.-H. Wu, K.-D. Tsuei, D.-J. Kim, Z. Fisk, A. Tanaka, P. Thalmeier, and L. H. Tjeng, *Phys. Rev. B* **96**, 155130 (2017).
- [27] V. B. Zabolotnyy, K. Fürsich, R. J. Green, P. Lutz, K. Treiber, C.-H. Min, A. V. Dukhnenko, N. Y. Shitsevalova, V. B. Filipov, B. Y. Kang, B. K. Cho, R. Sutarto, F. He, F. Reinert, D. S. Inosov, and V. Hinkov, *Phys. Rev. B* **97**, 205416 (2018).
- [28] V. Alexandrov, P. Coleman, and O. Erten, *Phys. Rev. Lett.* **114**, 177202 (2015).
- [29] O. Erten, P. Ghaemi, and P. Coleman, *Phys. Rev. Lett.* **116**, 046403 (2016).
- [30] A. Stern, M. Dzero, V. M. Galitski, Z. Fisk, and J. Xia, *Nat. Mater.* **16**, 708 (2017).
- [31] A. Barla, J. Derr, J. P. Sanchez, B. Salce, G. Lapertot, B. P. Doyle, R. Rüffer, R. Lengsdorf, M. M. Abd-Elmeguid, and J. Flouquet, *Phys. Rev. Lett.* **94**, 166401 (2005).
- [32] K. Nishiyama, T. Mito, G. Pristas, Y. Jara, T. Koyama, K. Ueda, T. Kohara, Y. Akahama, S. Gabani, M. Reiffers, K. Flachbart, H. Fukazawa, Y. Kohori, N. Takeshita, and N. Shitsevalova, *J. Phys. Soc. Jpn.* **82**, 123707 (2013).
- [33] W. T. Fuhrman, J. Leiner, P. Nikolić, G. E. Granroth, M. B. Stone, M. D. Lumsden, L. DeBeer-Schmitt, P. A. Alekseev, J.-M. Mignot, S. M. Koohpayeh, P. Cottingham, W. A. Phelan, L. Schoop, T. M. McQueen, and C. Broholm, *Phys. Rev. Lett.* **114**, 036401 (2015).
- [34] V. N. Gurin and M. M. Korsukova, *Prog. Cryst. Growth Charact.* **6**, 59 (1983).
- [35] V. N. Gurin and L. I. Derkachenko, *Progr. Cryst. Growth Charact. Mater.* **27**, 163 (1993).
- [36] W. G. Moffatt, *Handbook of Binary Phase Diagrams*, edited by J. H. Westbrook (Genium Publ., Amsterdam, New York, 2006).
- [37] B. Ravel and M. Newville, *J. Synchrotron Radiat.* **12**, 537 (2005).
- [38] P. Ohresser, E. Otero, F. Choueikani, K. Chen, S. Stanescu, F. Deschamps, T. Moreno, F. Polack, B. Lagarde, J.-P. Daguette,

- F. Marteau, F. Scheurer, L. Joly, J.-P. Kappler, B. Muller, O. Bunau, and Ph. Sainctavit, *Rev. Sci. Instrum.* **85**, 013106 (2014).
- [39] F. Baudelet, L. Nataf, and R. Torchio, *High Pres. Res.* **36**, 429 (2016).
- [40] E. Stavitski and F. M. F. de Groot, *Micron* **41**, 687 (2010).
- [41] M. Pompa, A. M. Flank, P. Lagarde, J. C. Rife, I. Stekhin, M. Nakazawa, H. Ogasawara, and A. Kotani, *Phys. Rev. B* **56**, 2267 (1997).
- [42] M. Mizumaki, S. Tsutsui, and F. Iga, *J. Phys.: Conf. Ser.* **176**, 012034 (2009).
- [43] J. Derr, G. Knebel, G. Lapertot, B. Salce, M.-A. Méasson, and J. Flouquet, *J. Phys. Condens. Matter* **18**, 2089 (2006).
- [44] J. C. Cooley, M. C. Aronson, Z. Fisk, and P. C. Canfield, *Phys. Rev. Lett.* **74**, 1629 (1995).
- [45] J. Derr, G. Knebel, D. Braithwaite, B. Salce, J. Flouquet, K. Flachbart, S. Gabáni, and N. Shitsevalova, *Phys. Rev. B* **77**, 193107 (2008).
- [46] S. S. Dhesi, P. Bencok, N. B. Brookes, G. van der Laan, and R. M. Galera, *J. Appl. Phys.* **93**, 8337 (2003).
- [47] S. S. Dhesi, G. van der Laan, P. Bencok, N. B. Brookes, R. M. Galera, and P. Ohresser, *Phys. Rev. B* **82**, 180402 (2010).
- [48] E.-M. Anton, B. J. Ruck, C. Meyer, F. Natali, H. Warring, F. Wilhelm, A. Rogalev, V. N. Antonov, and H. J. Trodahl, *Phys. Rev. B* **87**, 134414 (2013).
- [49] M. Bersweiler, K. Dumesnil, F. Wilhelm, and A. Rogalev, *Phys. Rev. B* **88**, 054411 (2013).
- [50] T. Jo, *J. Electron Spectrosc. Relat. Phenom.* **86**, 73 (1997).
- [51] R. D. dos Reis, L. S. I. Veiga, C. A. Escanhoela Jr., J. C. Lang, Y. Joly, F. G. Gandra, D. Haskel, and N. M. Souza-Neto, *Nat. Commun.* **8**, 1203 (2017).